Journal of Watershed Ecology

SCIEPublish

Article

Assessment of the Impact of Climate Change on Current and Future Runoff in the Nanija Bolong Watershed (Kaffrine Region, Senegal)

Modou Ndiaye * and Cheikh Faye

Department of Geography, Geomatics and Environment Laboratory, Faculty of Science and Technology, Assane Seck University of Ziguinchor, Ziguinchor 27000, Senegal; cheikh.faye@univ-zig.sn (C.F.)

* Corresponding author. E-mail: m.n220@zig.univ.sn (M.N.)

Received: 2 August 2026; Revised: 9 September 2026; Accepted: 9 October 2026; Available online: 26 October 2026

ABSTRACT: Climate change poses a major challenge to water-resource management in West Africa's Sudano-Sahelian regions. This study assesses projected changes in runoff in Senegal's Nanija Bolong catchment using ISIMIP3b outputs from two global hydrological models (H08 and Climate, Weather and Atmospheric Modeling (CWATM)) driven by three CMIP6 climate models (GFDL-ESM4, MPI-ESM1-2-HR, and MRI-ESM2-0). The analysis uses 1985–2014 as the historical reference period and 2021–2100 for future projections under SSP1-2.6, SSP3-7.0, and SSP5-8.5. Mann–Kendall, Sen's slope, and Pettitt tests were applied to the simulated series. The historical analysis shows no statistically significant trend in the simulated runoff series. Future changes differ in magnitude between H08 and CWATM and are not monotonic across scenarios in every time window: relative to 1985–2014, the late-century reductions under SSP3-7.0 are larger than under SSP5-8.5 in the ensemble series. Because a complete, independently documented observed Nanija Bolong discharge series was not available in the material used for this analysis, the study does not claim observational validation of either model. The results should therefore be interpreted as model-based projections and as an assessment of structural and climate-model uncertainty, not as proof that either model reproduces measured discharge accurately. The coarse spatial resolution also limits fine-scale interpretation within this small catchment.

Keywords: Climate change; Nanija Bolong catchment; Discharge; CMIP6; H08; CWATM

1. Introduction

Climate change is now one of the major challenges facing environmental systems and human societies. As a result of the continuous increase in atmospheric concentrations of greenhouse gases, the global average temperature has already risen by approximately 1.1 °C compared with the pre-industrial period, leading to an intensification of the hydrological cycle, changes in rainfall patterns, and an increase in the frequency and intensity of extreme hydrological events [1]. These changes directly affect the availability of water resources, the dynamics of catchment areas, and the ecological balances on which agricultural, industrial, and domestic activities depend. The scientific consensus on the reality of climate change and its anthropogenic origin is now widely established [2], whilst recent research highlights the need to improve

© 2026 The authors. This is an open access article under the Creative Commons Attribution 4.0 International License (https://creativecommons.org/licenses/by/4.0/).

our understanding of the interactions among climate, hydrology and human activities to develop effective adaptation strategies [3].

Water resources are particularly sensitive to climatic variations because they result from complex interactions among precipitation, evapotranspiration, soil moisture, surface runoff, and groundwater. Any change in these components directly influences the hydrological functioning of catchments and water availability at various spatial scales [4,5]. The expected changes concern not only annual runoff volumes, but also the seasonality of flows, low-water periods, floods, and groundwater recharge, with significant consequences for food security, hydroelectric power generation, aquatic ecosystems, and domestic water use [6].

In this context, catchment areas are key units for analysing the impacts of climate change on the water cycle. Rainfall–runoff models now make it possible to represent fundamental hydrological processes and to simulate catchment responses to future climate changes. Advances in hydrological modelling, particularly in calibration, data assimilation, and uncertainty quantification, have significantly improved the reliability of hydrological projections [7]. Global water resource models such as H08, PCR-GLOBWB, and CWATM now allow natural and anthropogenic processes—including water abstractions, irrigation, reservoirs, and agricultural uses—to be integrated into the assessment of climate impacts [8–10].

At the same time, recent research shows that future changes in river flows will depend heavily not only on the level of greenhouse gas emissions, but also on the specific characteristics of each catchment area. Several studies conducted in different climatic contexts thus highlight contrasting hydrological responses, with marked decreases in runoff in some catchments and an increased risk of flooding in others [11–13]. This diversity of hydrological responses underscores the need to develop regional studies based on multi-model approaches in order to better characterise uncertainties and improve the sustainable management of water resources.

West Africa is among the regions most vulnerable to the effects of climate change due to the population's heavy reliance on natural resources and the predominance of rain-fed agricultural activities. Since the major Sahelian droughts of the 1970s and 1980s, the region has experienced high hydroclimatic variability characterised by alternating years of water deficit and surplus, a gradual rise in temperatures, and an intensification of extreme rainfall events [14–16]. Climate projections indicate that this variability is likely to increase during the 21st century, with significant consequences for water resources, agricultural systems, and ecosystems [17,18].

In Senegal, climate observations indicate a continuous rise in temperatures and a shift in the seasonal distribution of rainfall, despite a relative recovery in rainfall since the early 1990s. This trend is reflected in high variability in river flows, an increase in flooding events, and persistent hydrological deficits in several catchment areas [19–21]. The Sudano-Sahelian basins appear particularly vulnerable due to their heavy reliance on seasonal rainfall and the significance of agro-pastoral activities.

The Nanija Bolong catchment, located in the Kaffrine region, perfectly illustrates this vulnerability. Its hydrological functioning depends primarily on winter rains, whilst changes in land use, degradation of vegetation cover, overgrazing, and agricultural expansion are gradually altering the processes of runoff, infiltration, and groundwater recharge [22,23]. Against this backdrop, assessing the future impacts of climate change is a major challenge for integrated water resources management and the planning of hydro-agricultural developments, in line with the guidelines of the Kayanga-Géba Basin IWRM Action Plan [24].

Recent advances in climate modelling now offer new perspectives for studying these impacts. The sixth phase of the Coupled Model Intercomparison Project (CMIP6) significantly improves the representation of atmospheric and oceanic processes as well as climate feedbacks [25,26]. Simulations based on Socio-Economic Scenarios (SSPs) enable the exploration of different climate futures, whilst the ISIMIP project harmonises projections from multiple climate models using robust bias correction and statistical disaggregation procedures [27,28]. Several studies have also demonstrated the strong performance of CMIP6 models in reproducing African rainfall patterns [29] and West African monsoon rainfall [18]. Despite these

advances, studies focusing on small catchments in central Senegal remain few in number, leaving significant uncertainties regarding the future impacts of climate change on local water resources.

Improved climate projections must be accompanied by a reliable representation of hydrological processes to convert climate variables into indicators directly usable for water resource management. The H08 and CWATM global hydrological models meet this objective by simulating the main processes of the hydrological cycle, including runoff, infiltration, evapotranspiration, groundwater flow, and routing within the river network [8,30,31]. The simultaneous use of multiple hydrological and climate models is now a recognised approach to better represent the uncertainties inherent in future projections and enhance the robustness of the results [32,33].

The analysis of hydrological time series also relies on robust statistical methods that enable trends to be identified, their intensity to be estimated, and any breaks in the flow time series to be detected. The non-parametric Mann-Kendall, Sen's slope, and Pettitt tests are widely used to characterise hydroclimatic changes at different spatial scales [34,35]. These approaches provide a methodological framework particularly well-suited to studying the impacts of climate change on water resources, particularly in regions where hydrometric observations remain limited.

Several recent studies carried out in Senegal have already confirmed the sensitivity of catchment areas to climate change. Studies carried out on the Casamance, Kayanga-Géva, Agua-Foua-Djilass, and Gambia River catchments highlight a gradual decline in water resources, an increase in the frequency of hydrological droughts, and a change in the characteristics of future flows under CMIP6 scenarios [36–42]. However, despite these advances, the Nanija Bolong catchment remains very poorly documented, even though it represents a strategic area for agricultural development and food security in central Senegal.

This lack of knowledge limits the ability of managers and decision-makers to anticipate the future effects of climate change on water resource availability and to incorporate this information into policies on hydro-agricultural development, risk prevention, and integrated water resources management. It therefore appears essential to produce robust hydrological projections at the scale of this catchment in order to better characterise its future evolution.

This study, therefore, assesses model-simulated runoff changes in the Nanija Bolong catchment using a harmonised multi-model framework. It has three objectives: (i) to characterise simulated historical runoff over 1985–2014; (ii) to quantify projected changes over 2021–2100 under SSP1-2.6, SSP3-7.0, and SSP5-8.5; and (iii) to compare the response of H08 and CWATM while reporting uncertainty across the three climate models. This study is not presented as a calibration or observation-based validation, as the Nanija Bolong watershed is an ungauged basin.

2. Materials and Methods

2.1. Study Area

The Nanija Bolong catchment is situated on the border between the Tambacounda and Kaffrine regions. Centred around its main branch, the Nanija Bolong is a 208 km long watercourse that drains a catchment area of approximately 3700 km^2. The outlet, the catchment polygon, and the selected model grid cells were checked for mutual spatial consistency: the outlet lies at the downstream end of the catchment, and the retained grid cells (Figure 1) fall within the catchment bounding box. Longitude is expressed in decimal degrees west as negative values. This documented internal-consistency check is the explicit basis for the selection; no additional external GIS layer was available, so any residual uncertainty is carried into the interpretation, and all results are read at model-grid scale. Administratively, the catchment spans several territorial units, including Kouthia, Gaydi, Kouthiaba Ouolof, Maléme Niani, Mareto, Pass Koto, Fass Thiekene, Ida Mouride, Koungheul, Koumpentou, Ndame, and Saly Escale.

The catchment has a generally undulating topography, with altitudes ranging from 60 m upstream to 4 m downstream, which encourages concentrated runoff and poses a risk of gully erosion in the absence of appropriate management measures. It is one of the catchment areas showing early signs of significant development, with 300 hectares under cultivation, comprising 135 hectares on the left bank and 165 hectares on the right bank.

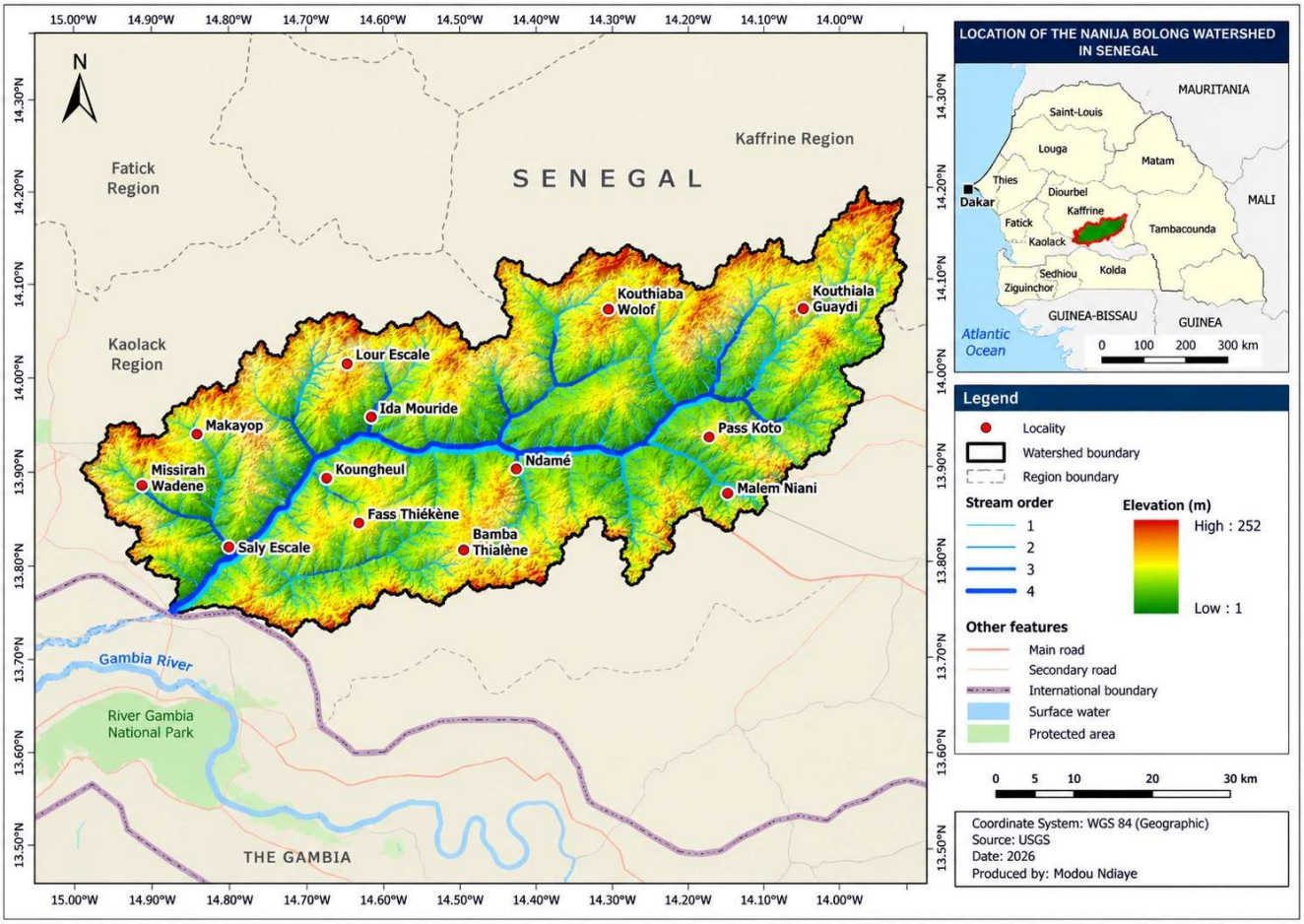


Figure 1. Location of the Nanija Bolong catchment.

2.2. Hydrological Data

To assess model-simulated runoff changes in the Nanija Bolong catchment, we used outputs from the Inter-Sectoral Impact Model Intercomparison Project (ISIMIP). The previous reference to the Nanija Bolong catchment was an error carried over from another text and has been removed. ISIMIP3b provides harmonised climate and hydrological simulations [27,28]. The climate forcing is supplied on a 0.5° × 0.5° grid after bias correction and statistical disaggregation. We extracted the grid cell or cells intersecting the Nanija Bolong catchment and the routed outlet series as provided by the source product; no fine-scale observations or catchment downscaling are implied. The outlet and grid-cell selection was verified for internal consistency against the catchment polygon and the ISIMIP file metadata (variable, model, scenario, and grid identifiers): the routed outlet series corresponds to the downstream-most 0.5° cell within the catchment, and the selected cells are those intersecting the catchment polygon. Because the catchment is ungauged, this verification is limited to spatial and metadata consistency; it is explicitly acknowledged that no independent gauged reference exists, and the coarse resolution is treated as a limitation in the Discussion.

2.2.1. H08 Model

H08 is a global hydrological model that incorporates natural and anthropogenic hydrological processes at a spatial resolution of 0.5° and a temporal resolution of 1 day [8]. The daily time step is useful for representing simulated event timing, but the 0.5° grid is coarse relative to the Nanija Bolong catchment. H08 is therefore used here primarily for basin-scale projection and model intercomparison, not for fine-scale local discharge estimation. No sub-grid interpolation or downscaling is assumed unless explicitly documented in the archived processing files [30].

2.2.2. CWATM Model

The Community Water Model (CWATM) is a distributed hydrological model developed by the European Commission's Joint Research Centre (JRC) as part of the Global Flood Awareness System (GloFAS). It simulates the main processes of the hydrological cycle at both catchment and global scales, including precipitation, evapotranspiration, infiltration, soil moisture, surface and groundwater flow, and the routing of flows within the river network. Thanks to its modular structure and flexible spatial resolution, CWATM enables the interactions between hydrological processes and human activities to be represented consistently. The model is widely used for water resource assessment, hydrological risk analysis, and the study of climate change impacts at various scales. As part of the ISIMIP3 project, CWATM is driven by several global climate models to produce consistent hydrological projections under different climate scenarios. These simulations enable the assessment of future changes in flow, water availability, and hydrological extremes, whilst quantifying the uncertainties associated with climate forcing and hydrological models [31,32].

2.2.3. Simulations Using Both Models

For each of the two hydrological models, H08 and CWATM, simulations were carried out using data from three global climate models (GCMs) from the sixth phase of the Coupled Model Intercomparison Project (CMIP6): GFDL-ESM4, MPI-ESM1-2-HR, and MRI-ESM2-0. These climate models were selected due to their widespread use in climate change impact studies and their ability to reproduce the main characteristics of the climate in West Africa. Before being used in ISIMIP, their climate outputs undergo a harmonised process of bias correction and statistical disaggregation (ISIMIP3BASD), ensuring greater consistency among the models and a more realistic representation of the meteorological variables that are used to drive the hydrological models.

The use of multiple climate models is intended to expose, rather than conceal, projection uncertainty. In the revised analysis, the ensemble mean is reported together with the range or standard deviation across the three GCM-driven simulations. Averaging is treated as a summary statistic; it is not, by itself, evidence that the projections are robust or that the individual models agree. The spread is reported explicitly in Table 1 (mean, standard deviation, and max–min range across the three GCM-driven simulations) for the historical period. For future periods, the statistics in Tables 2 and 3 are computed on the GCM-averaged series; the per-GCM future series are archived and available as stated in the Data Availability Statement.

The simulations cover a historical reference period (1985–2014) and the future period 2021–2100 under SSP1-2.6, SSP3-7.0, and SSP5-8.5. Future results are summarised for 2021–2040, 2041–2060, 2061–2080, and 2081–2100. Percentage changes are calculated relative to the 1985–2014 historical mean using $100 \times (Q_{future} - Q_{1985–2014})/Q_{1985–2014}$. The historical climate forcing is not treated as an observed discharge record. A formal measured-versus-modelled validation would require a complete and independently documented Nanija Bolong discharge series, including station metadata, units, and quality-control information; such a series was not available in the data package used here. The evaluation of hydrological model performance through comparisons between observed and simulated discharge, as

discussed in the hydrological modelling literature [7,30,31], is therefore recommended as a future step rather than presented as an analysis performed in the present study.

Table 1. Mann–Kendall and Pettitt tests on simulated discharge over the historical reference period (1985–2014) in the Nanija Bolong catchment (values are model/GCM-specific and are not observed-discharge validation metrics).

	Mann–Kendall Test				Pettitt Test				
Parameters	**Kendall's Tau**	***p*-Value**	**Alpha**	**Sen's Slope**	**Break Date**	***p*-Value**	**Mean Before Break**	**Mean After Break**	**Rate of Change (%)**
H08/MRI-ESM2-0	−0.0659	0.5541	0.05	−0.0116	2006	0.2578	13.61	15.71	+15.43
H08/MPI-ESM1-2-HR	0.1171	0.2881	0.05	0.0261	1992	0.4617	15.21	16.26	+6.93
H08/GFDL-ESM4	0.1244	0.2586	0.05	0.0197	1995	0.3817	13.87	15.55	+12.11
H08 ensemble mean	0.1415	0.1980	0.05	0.0158	1993	0.2285	14.23	15.83	+11.25
H08–SD of GCMs	0.1038	0.1264	0.00	0.0194	5.72	0.1036	0.72	0.38	4.33
H08–MCG range (Max–Min)	0.1903	0.2955	0	0.0377	14	0.2040	1.60	0.71	8.50
CWATM/MRI-ESM2-0	−0.0049	0.9733	0.05	−0.0045	1989	0.8914	16.83	16.66	−1.00
CWATM/MPI-ESM1-2-HR	0.1488	0.1754	0.05	0.127	2001	0.1588	15.15	18.37	+21.27
CWATM/GFDL-ESM4	0.0951	0.3897	0.05	0.1287	1991	0.7517	16.55	17.44	+5.36
CWATM ensemble mean	0.2073	0.0574	0.05	0.0990	1993	0.2654	16.35	18.12	+10.82
CWATM–SD of GCMs	0.0778	0.3286	0.00	0.0598	5.35	0.3078	0.86	0.73	9.05
CWATM–MCG range (Max–Min)	0.1537	0.7979	0	0.1332	12	0.7326	1.68	1.81	22.27

The rate of change is expressed as a percentage of the flow rate.

Table 2. Statistics on the flow simulated by H08 and CWATM for the future period based on future projections of the three CMIP6 GCMs used (GFDL-ESM4, MPI-ESM1-2-HR, MRI-ESM2-0) in the Nanija Bolong catchment.

SSP 126/MCG/H08	**1985–2014**	**2021–2040**	**2041–2060**	**2061–2080**	**2081–2100**	**2021–2100**
H08/MRI-ESM2-0	3.5	5.4	5.6	2.8	2.0	3.8
H08/MPI-ESM1-2-HR	3.8	2.8	3.9	2.5	3.1	3.2
H08/GFDL-ESM4	4.3	1.8	3.2	3.0	3.0	3.0
Average	3.8	3.3	4.2	2.8	2.7	3.4
Standard deviation	0.4	1.8	1.2	0.2	0.6	0.4
MCG range (Max–Min)	0.8	3.5	2.3	0.5	1.1	0.8
SSP 126/MCG/CWATM	**1985–2014**	**2021–2040**	**2041–2060**	**2061–2080**	**2081–2100**	**2021–2100**
H08/MRI-ESM2-0	17.3	21.6	20.9	15.5	13.9	17.9
H08/MPI-ESM1-2-HR	16.1	15.2	17.0	12.7	15.4	15.3
H08/GFDL-ESM4	18.2	11.7	15.7	14.7	16.2	15.3
Average	17.2	16.2	17.9	14.3	15.2	16.1
Standard deviation	1.0	5.1	2.7	1.4	1.2	1.5
MCG range (Max–Min)	2.1	10.0	5.3	2.8	2.4	2.6
SSP 370/MCG/H08	**1985–2014**	**2021–2040**	**2041–2060**	**2061–2080**	**2081–2100**	**2021–2100**
H08/MRI-ESM2-0	3.5	4.4	2.1	3.1	0.5	2.7
H08/MPI-ESM1-2-HR	3.8	4.2	4.9	1.5	0.8	3.0
H08/GFDL-ESM4	4.3	2.4	1.2	1.7	1.0	2.1
Average	3.8	3.7	2.7	2.1	0.8	2.6
Standard deviation	0.4	1.1	1.9	0.9	0.2	0.5
MCG range (Max–Min)	0.8	2.0	3.7	1.6	0.4	0.9
SSP 370/MCG/CWATM	**1985–2014**	**2021–2040**	**2041–2060**	**2061–2080**	**2081–2100**	**2021–2100**
H08/MRI-ESM2-0	17.3	18.1	16.5	13.1	6.0	14.2
H08/MPI-ESM1-2-HR	16.1	19.8	19.6	12.4	9.9	15.6

H08/GFDL-ESM4	18.2	14.5	9.0	9.4	9.0	12.0
Average	17.2	17.5	15.1	11.6	8.3	13.9
Standard deviation	1.0	2.7	5.5	1.9	2.1	1.8
MCG range (Max–Min)	2.1	5.3	10.6	3.6	3.9	3.5
SSP 585/MCG/H08	**1985–2014**	**2021–2040**	**2041–2060**	**2061–2080**	**2081–2100**	**2021–2100**
H08/MRI-ESM2-0	3.5	6.2	4.1	0.7	0.5	3.0
H08/MPI-ESM1-2-HR	3.8	3.9	2.4	1.5	2.0	2.7
H08/GFDL-ESM4	4.3	2.3	2.1	2.0	1.1	2.3
Average	3.8	4.1	2.9	1.4	1.2	2.7
Standard deviation	0.4	2.0	1.1	0.6	0.8	0.3
MCG range (Max–Min)	0.8	3.9	1.9	1.2	1.6	0.6
SSP 585/MCG/CWATM	**1985–2014**	**2021–2040**	**2041–2060**	**2061–2080**	**2081–2100**	**2021–2100**
H08/MRI-ESM2-0	17.3	22.6	17.5	8.3	5.8	14.3
H08/MPI-ESM1-2-HR	16.1	17.0	14.3	13.4	13.2	14.8
H08/GFDL-ESM4	18.2	14.6	15.0	14.8	12.0	14.9
Average	17.2	18.1	15.6	12.2	10.3	14.7
Standard deviation	1.0	4.1	1.7	3.4	4.0	0.3
MCG range (Max–Min)	2.1	8.1	3.3	6.4	7.5	0.6

Table 3. Mann–Kendall and Pettitt tests based on simulated discharge from H08 and CWATM over 2021–2100 in the Nanija Bolong catchment. Percent changes compare the pre- and post-break means within each simulated series.

Parameters		Man-Kendall Test				Pettitt's Test				
		Kendall's Tau	*p*-Value (Two-Tailed)	Alpha	Sen's Slope	Date of Failure	*p*-Value	Mean Before Break	Mean After Break	Rate of Change
Simulated flow rates (H08)	SSP 126	−0.1899	0.0128	0.05	−0.01209	2061	0.0092	3.780	2.730	−027.77
	SSP 370	−0.6184	<0.0001	0.05	−0.03705	2067	<0.0001	3.298	0.979	−070.32
	SSP 585	−0.5348	<0.0001	0.05	−0.03972	2065	<0.0001	3.410	1.152	−066.21
Simulated flow rates (CWATM)	SSP 126	−0.1323	0.0832	0.05	−0.03951	2065	0.0647	16.943	14.574	−013.98
	SSP 370	−0.4665	<0.0001	0.05	−0.14870	2067	<0.0001	16.039	9.169	−042.83
	SSP 585	−0.3709	<0.0001	0.05	−0.12624	2065	<0.0001	16.999	10.436	−038.61

The rate of change is expressed relative to the 1985–2014 historical reference mean. Future sub-periods are 2021–2040, 2041–2060, 2061–2080, and 2081–2100.

3. Results

3.1. Trends in Discharge

Simulation and Estimation of Discharge Rates over the Historical Period

Table 1 presents Mann–Kendall, Sen slope, and Pettitt results for the simulated discharge series. To avoid mixing incompatible averages, the historical reference period for the period-comparison analysis is 1985–2014 throughout the revised manuscript. The statistics in Table 1 are computed from the same annual series and the same aggregation procedure as those used for Table 3, so the historical reference is homogeneous throughout the manuscript.

Analysis of the Mann-Kendall test shows that the Kendall coefficients (τ) remain relatively low across all simulations. For the H08 model, the values range from −0.0659 (MRI-ESM2-0) to 0.1415 (GCM average), whilst those for the CWATM model range from −0.0049 (MRI-ESM2-0) to 0.2073 (GCM average). These low coefficients reflect the absence of a marked trend in discharge rates over the period studied. Furthermore, the *p*-values associated with the Mann-Kendall test are all above the 5% significance threshold ($\alpha = 0.05$). Consequently, the null hypothesis of no trend cannot be rejected. The variations observed over the historical period, therefore, correspond more to natural climate variability than to a statistically significant change in the hydrological regime.

Estimates of Sen's slope confirm this interpretation. The values obtained remain low, reflecting slow changes in flow rates. For the H08 model, the slopes range from −0.0116 to 0.0261 m^3/s per year, whilst for CWATM they reach up to 0.1287 m^3/s per year. The positive slopes observed for the majority of simulations indicate a slight increase in flow rates over the historical period, whilst the few negative values (H08/MRI-ESM2-0 and CWATM/MRI-ESM2-0) indicate a slight local decrease. However, given the lack of statistical significance in the Mann-Kendall test, these trends should be interpreted with caution and do not reflect a lasting change in the hydrological regime.

The Pettitt test, used to identify a possible break in the time series, highlights dates of change ranging from 1989 to 2006, depending on the models and GCMs. For H08, breaks are mainly detected between 1992 and 2006, whilst CWATM identifies breaks between 1989 and 2001. However, the *p*-values from the Pettitt test are all greater than 0.05, indicating that these breaks are not statistically significant. They probably correspond to interannual or decadal fluctuations linked to climatic events characteristic of West Africa, notably the droughts of the 1970s and 1980s, followed by a partial recovery in rainfall in the 1990s and 2000s.

The model-specific historical means in this table should not be compared directly with the values in Table 3 unless they are calculated from the same series and aggregation procedure. We therefore interpret the historical results only as evidence of weak or non-significant trends in the simulated series, not as observational validation.

The additional uncertainty metrics reported in Table 1 highlight the inter-GCM variability in the historical simulated discharge trends for both hydrological models. For H08, Kendall's tau ranges from −0.0659 to 0.1244, while the post-break rate of change varies from +6.93% to +15.43% among the three GCMs. For CWATM, Kendall's tau ranges from −0.0049 to 0.1488, and the post-break rate of change extends from −1.00% to +21.27%. These ranges indicate that the historical trend signal remains weak and that its magnitude depends on the selected climate model. The ensemble mean alone may therefore mask part of the variability between individual GCM-driven simulations. To better represent this uncertainty, Table 1 now includes both the standard deviation (SD) and the min–max range of the three GCM simulations for each hydrological model. The relatively small SD values for Kendall's tau (0.1038 for H08 and 0.0778 for CWATM) confirm limited dispersion in trend direction, whereas the larger ranges observed for Sen's slope and rate of change indicate greater uncertainty in the magnitude of simulated variations. For the future periods (Tables 2 and 3), the statistics are computed on the GCM-averaged series, and the per-GCM series are archived (see Data Availability Statement).

The two models produce different absolute flows, with CWATM generally higher than H08. This difference is consistent with alternative representations of runoff generation, infiltration, storage, evapotranspiration, and routing, but the present analysis does not identify which formulation is more accurate because no independently documented observed discharge series was available. Agreement between the models is therefore treated as model intercomparison, not validation.

The 1985–2014 period is used as the common historical reference against which future simulated changes are calculated.

Figure 2 does not demonstrate that either model reproduces observed catchment behaviour. The H08 rainfall–simulated-flow relationship is weak (R^2 = 0.1246), while the CWATM relationship is stronger (R^2 = 0.7675); these statistics describe associations within the simulations and should not be interpreted as performance metrics against measured discharge.

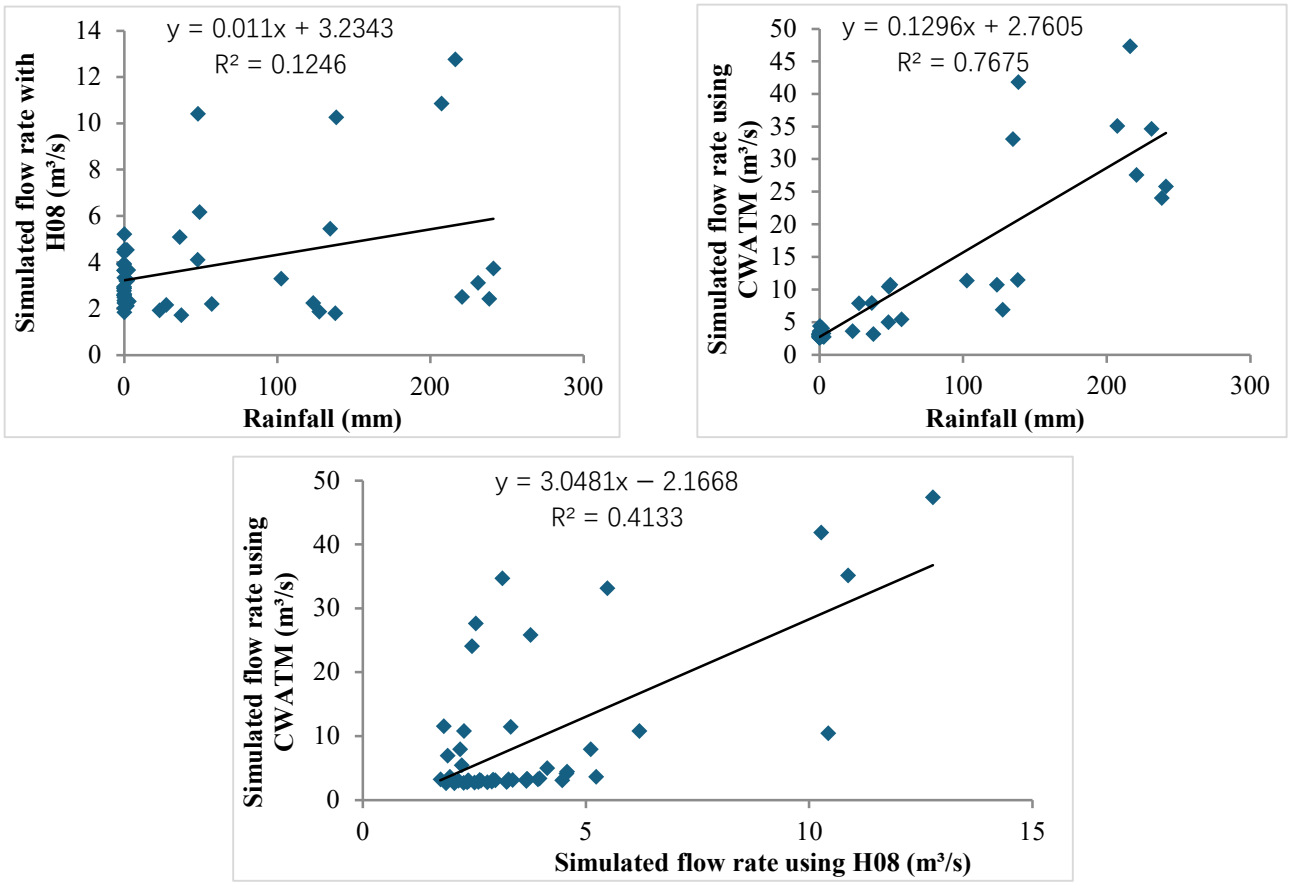


Figure 2. Association between rainfall and simulated discharge from the H08 and CWATM models over the historical reference period (1985–2014) at the Nanija Bolong outlet. The figure compares model variables; it is not an observed-versus-modelled validation.

At the global scale, recent assessments have further highlighted substantial past and projected changes in river flows, emphasizing the importance of accounting for regional differences and uncertainties in hydrological projections [43].

A direct comparison of the two models reveals substantial differences in simulated volume and variability. These differences are retained as an important component of hydrological-model uncertainty.

The evaluations of CWATM by Burek et al. [31] and of H08 by Hanasaki et al. [8,30] were performed in gauged basins elsewhere and cannot be transferred to the ungauged Nanija Bolong catchment. Accordingly, no accuracy ranking between the two models is claimed here; their differences are used only to bracket structural uncertainty. This is consistent with studies conducted in West Africa showing that the performance of hydrological models depends heavily on their ability to represent runoff, infiltration, and water-storage processes [44,45].

The simulations indicate that rainfall is an important driver of the modelled seasonal runoff, but the strength of this relationship and the absolute flow magnitude remain model-dependent. No validation by observation was carried out due to the absence of measured runoff, the Nanija Bolong catchment being ungauged.

Figure 3 shows the average monthly hydrographs simulated by the H08 and CWATM hydrological models, as well as the trend in average monthly rainfall over the historical period (1985–2014) at the outlet of the Nanija Bolong catchment. This representation enables an analysis of the catchment's seasonal behaviour, the synchronisation between rainfall and runoff, and the ability of the two models to reproduce the hydrological dynamics characteristic of Sudano-Sahelian catchments.

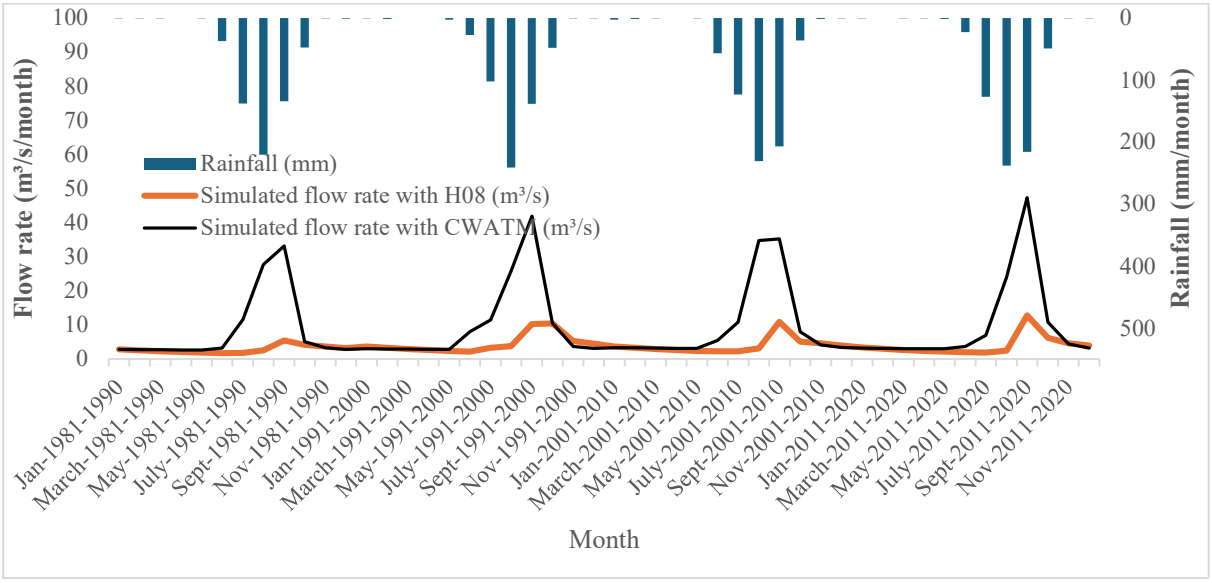


Figure 3. Monthly hydrographs simulated by H08 and CWATM over the historical reference period (1985–2014) at the outlet of the Nanija Bolong catchment.

The figure clearly highlights a strong seasonality in runoff, directly linked to the region's monomodal rainfall pattern. Discharge remains very low for most of the year, particularly from November to June, a period corresponding to the dry season. During this period, rainfall is virtually nil, and the observed discharge results mainly from water reserves stored in the soil and surface water tables. The simulated values, therefore, remain below a few cubic metres per second, reflecting the temporary and poorly fed nature of the basin's river network.

From July onwards, the first rains of the wet season lead to a gradual increase in flow rates. This rise in water levels continues throughout August and September, which corresponds to the period of heavy rainfall in West Africa. The hydrographs show that discharge rates peak during this period, before gradually decreasing from October onwards as the rainy season draws to a close. This pattern reflects a relatively rapid hydrological response of the catchment to rainfall, a characteristic of small tropical catchments where surface runoff constitutes a significant component of the flow.

However, a comparative analysis of the two models reveals significant differences in the intensity of the simulated discharge rates. The CWATM model produces much higher flood peaks than the H08 model, particularly during August and September. This difference is consistent with the structures of the two models: CWATM is a distributed model that represents in detail the processes of runoff, infiltration, groundwater flow, and routing, whilst H08 adopts a more global approach that incorporates the effects of storage and flow regulation to a greater extent.

A comparison of the hydrographs and rainfall data also highlights good synchronisation between the two variables. Peak flows occur immediately after rainfall maxima, reflecting the catchment's low hydrological inertia. This rapid response can be explained by several physical characteristics of the Nanija Bolong catchment, notably its relatively small area, short flow concentration times, and the presence of soils whose saturation capacity is quickly reached during intense rainfall events. However, the amplitude of the discharge remains lower than that of precipitation, indicating that a significant proportion of the rainwater is lost through infiltration, evapotranspiration, or temporary storage in natural depressions before entering the river system.

The hydrographs also highlight the regulatory role of the catchment's water reserves. After the end of the rainy season, discharge rates decrease gradually without ceasing immediately. This decline reflects the contribution of groundwater flow and soil water reserves, which continue to feed the watercourses for

several weeks after rainfall has stopped. This phenomenon is more pronounced in the CWATM simulations, which explicitly represent surface water–groundwater exchanges; whether this yields more accurate base flows cannot be assessed here because no observed discharge is available.

The two models reproduce a similar simulated seasonal timing, but this agreement should not be described as an accurate reproduction of the observed catchment regime. The figure shows model behaviour only; observed discharge is not included.

These observations are consistent with the work of Burek et al. [31] on the CWATM model, Hanasaki et al. [30] for the H08 model, as well as that of Sadio et al. [39,40] and Dione and Faye [36], which show that West African catchments exhibit a highly seasonal hydrological regime, dominated by winter rainfall and particularly sensitive to the effects of climate change.

3.2. Simulation and Estimation of Runoff over the Future Period

3.2.1. Annual Trends

Table 2 presents the evolution of simulated flow rates in the Nanija Bolong catchment under the three CMIP6 scenarios (SSP1-2.6, SSP3-7.0, and SSP5-8.5), using the H08 and CWATM hydrological models forced by three GCMs (MRI-ESM2-0, MPI-ESM1-2-HR, and GFDL-ESM4). The results highlight a general decrease in future runoff, although the magnitude of the reduction varies according to the hydrological model, emission scenario, and climate model used.

For the H08 model, the ensemble mean indicates a moderate decline under SSP1-2.6, with discharge decreasing from 3.8 m^3/s during the historical period to 2.7 m^3/s by 2081–2100. Under SSP3-7.0 and SSP5-8.5, the reduction becomes more pronounced, reaching 0.8 m^3/s and 1.2 m^3/s, respectively, at the end of the century. These results suggest a stronger drying signal under higher-emission scenarios. However, the inter-GCM uncertainty remains noticeable, particularly during the near-term period (2021–2040), where the range reaches 3.5 m^3/s under SSP1-2.6 and 3.9 m^3/s under SSP5-8.5.

The CWATM model simulates substantially higher flow rates than H08 throughout all scenarios, reflecting structural differences between the two hydrological models. Nevertheless, CWATM shows the same long-term downward tendency. Under SSP3-7.0, the ensemble mean decreases from 17.2 m^3/s historically to 8.3 m^3/s during 2081–2100, while SSP5-8.5 leads to a reduction to 10.3 m^3/s. The largest uncertainty among GCMs is observed under SSP3-7.0, particularly during 2041–2060, with a maximum–minimum range of 10.6 m^3/s.

Overall, the comparison between models confirms a consistent future reduction in runoff, while the magnitude of change remains dependent on both hydrological model structure and climate forcing uncertainty. The inclusion of standard deviation and MCG range provides a clearer representation of projection uncertainty and avoids interpreting the ensemble mean alone as a complete representation of future hydrological responses.

Table 3 presents the results of the Mann-Kendall, Sen's slope, and Pettitt tests applied to the discharge data simulated by the H08 and CWATM hydrological models under the three CMIP6 climate scenarios (SSP1-2.6, SSP3-7.0, and SSP5-8.5) over the period 2021–2100.

Analysis of the Mann-Kendall test reveals a trend that differs significantly from that observed during the historical period. Unlike the historical results, where no significant trend was detected, the future simulations show widespread negative trends, indicating a gradual decrease in discharge rates over the course of the 21st century. The Kendall coefficients (τ) are all negative, regardless of the model-scenario combination, reflecting a downward trend in flows. The values range from −0.1323 to −0.6184, with the strongest value (−0.6184) observed for H08 under SSP3-7.0. This gradual decline suggests that surface water resources are likely to become increasingly limited as climate change intensifies.

The *p*-values confirm the robustness of these results. Under the SSP126 scenario, only the H08 simulation shows a statistically significant trend ($p = 0.0128$), whilst that of CWATM ($p = 0.0832$) remains slightly above the 5% threshold, indicating a still moderate decrease in the context of reduced greenhouse gas emissions. By contrast, under the SSP370 and SSP585 scenarios, both models show *p*-values below 0.0001, demonstrating a highly significant trend towards reduced flows. These results show that the decline is highly significant under both SSP3-7.0 and SSP5-8.5. However, the magnitude of the reduction is not ordered by emissions level in every period: SSP3-7.0 produces larger late-century reductions than SSP5-8.5 in the ensemble series (see Table 4), so no general emissions–reduction monotonicity is claimed.

Estimating the Sen's slope allows us to measure the rate of this decline. The slopes are consistently negative, confirming a gradual decline in flow rates over the years. For the H08 model, these slopes range from −0.01209 m^3/s/year under SSP126 to −0.03972 m^3/s/year under SSP585. The SSP370 scenario also shows a significant slope (−0.03705 m^3/s/year), very close to that obtained under SSP585. For the CWATM model, the decreases are even more pronounced in absolute terms, with rates of decline reaching −0.14870 m^3/s/year under SSP370 and −0.12624 m^3/s/year under SSP585. These results show that flows decline continuously throughout the century in all scenarios. The steepest Sen slope is not found under the highest-emission scenario for both models (for CWATM, −0.14870 m^3/s/year under SSP3-7.0 versus −0.12624 m^3/s/year under SSP5-8.5), so the decline is not described as accelerating with the emissions level.

The Pettitt test highlights significant breaks in the time series of future flow rates. The dates of these breaks are mainly between 2061 and 2067, regardless of the model–scenario combination. Under SSP370 and SSP585, the *p*-values are less than 0.0001, indicating that these breaks are statistically highly significant. These results suggest that the Nanija Bolong catchment could experience a significant change in its hydrological behaviour from the mid-21st century onwards. This period likely corresponds to the time when the cumulative effects of rising temperatures, increased evapotranspiration, and changes in the rainfall regime will become significant enough to cause a sustained reduction in runoff.

An analysis of the average flow rates before and after the breach illustrates the extent of these changes. For the H08 model, the average flow rate decreases from 3.78 to 2.73 m^3/s under SSP126, from 3.30 to 0.98 m^3/s under SSP370, and from 3.41 to 1.15 m^3/s under SSP585. The rates of change are −27.77%, −70.32% and −66.21% respectively. These results show very large reductions under both SSP3-7.0 (−70.32%) and SSP5-8.5 (−66.21%), the SSP3-7.0 reduction being slightly larger for H08. The responses are therefore period- and scenario-specific rather than a simple monotonic function of the emissions level.

The CWATM model confirms this general trend, whilst simulating less pronounced decreases. Average flows decrease from 16.94 to 14.57 m^3/s under SSP126, from 16.04 to 9.17 m^3/s under SSP370, and from 17.00 to 10.44 m^3/s under SSP585. The decreases amount to −13.98%, −42.83% and −38.61% respectively. Although CWATM produces higher absolute values than H08, both models agree on a significant decrease during the 21st century under SSP3-7.0 and SSP5-8.5. For CWATM as well, the decrease under SSP3-7.0 (−42.83%) exceeds that under SSP5-8.5 (−38.61%), confirming that the scenario ranking is not monotonic in emissions.

The difference between H08 and CWATM is treated as structural hydrological-model uncertainty. Plausible sources include different formulations of runoff generation, infiltration, soil and groundwater storage, evapotranspiration, river routing, grid aggregation, and human-water-use processes. These mechanisms are not separately tested here, so they are presented as possible explanations rather than demonstrated causes.

These results are consistent with numerous studies carried out in West Africa, which show a gradual decline in flows in the main catchment areas as a result of climate change. The work by Sadio et al. [39,40] on the Casamance and Kayanga catchments, that by Dione and Faye [36] on the Agua-Foua-Djilass catchment, as well as the simulations carried out using CWATM [31] and the ISIMIP multi-model

ensembles [32] all reach similar conclusions, highlighting a gradual reduction in water resources, particularly under high-emission scenarios.

Figure 4 shows annual simulated discharge from H08 and CWATM for the historical reference period (1985–2014) and the future period (2021–2100) under SSP1-2.6, SSP3-7.0, and SSP5-8.5.

Analysis of the historical period shows that the flows simulated by both models remain relatively stable, with interannual fluctuations primarily reflecting the natural variability of precipitation. Both models show similar simulated seasonal timing of the alternation between wet and dry years without revealing any marked long-term trend. During the first period (2021–2040), the differences between the scenarios remain relatively limited. Under SSP1-2.6, flows remain close to those observed during the historical period, reflecting the positive effects of a global policy to reduce greenhouse gas emissions. Under SSP3-7.0 and SSP5-8.5, variations remain moderate, although the first decreases are beginning to appear.

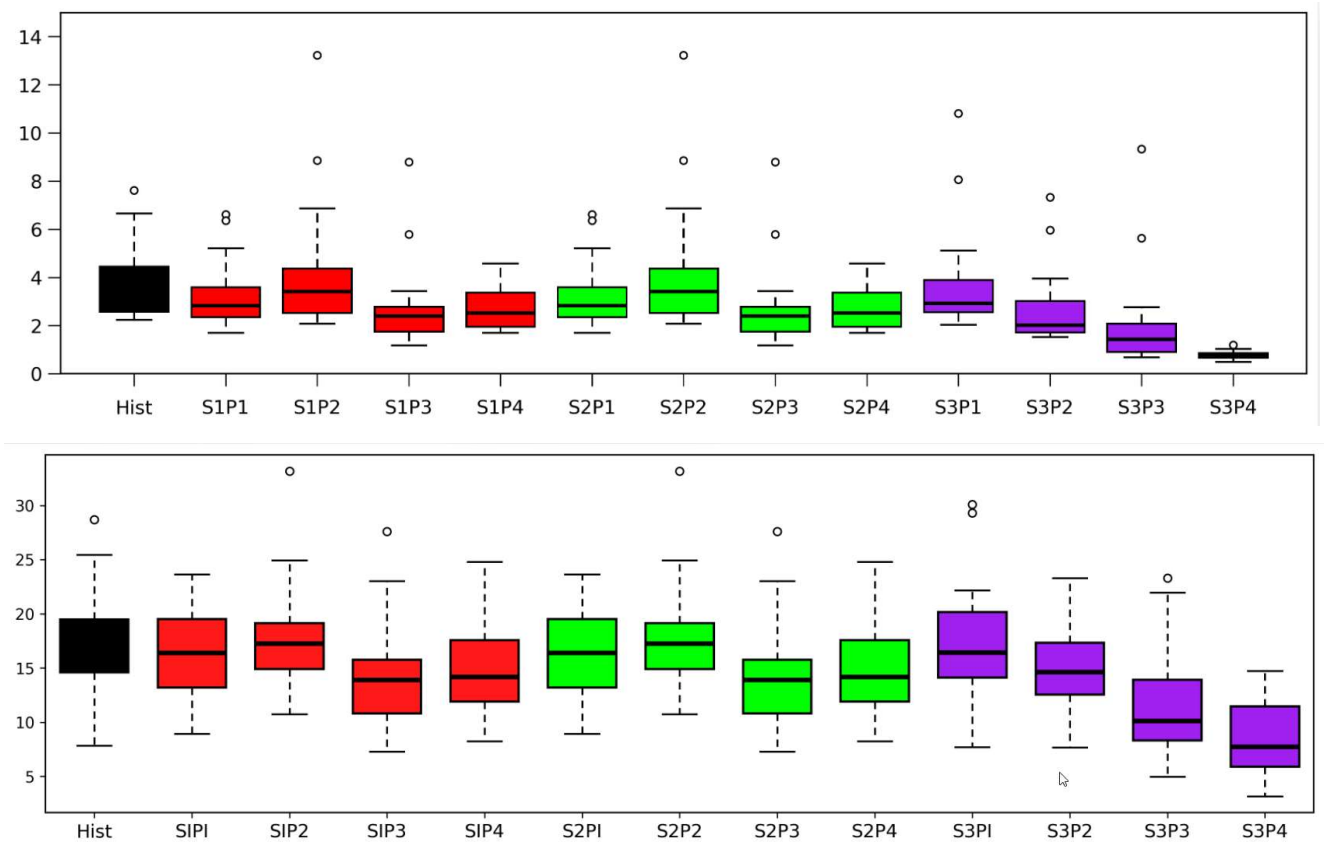


Figure 4. Annual simulated discharge over the historical reference period (1985–2014) and the future period (2021–2100) in the Nanija Bolong catchment.

From the 2040s–2050s onwards, the differences between the scenarios become much more pronounced. Under the SSP1-2.6 scenario, flows show some fluctuations but remain relatively stable, with a moderate decrease. In contrast, the SSP3-7.0 and SSP5-8.5 scenarios show a gradual and continuous decline in flows.

The decline becomes particularly marked after 2060, a period which also corresponds to the breakpoints identified by the Pettitt test in Table 3. From this point onwards, the curves for the SSP370 and SSP585 scenarios show a rapid and continuous decline until the end of the century. Under these scenarios, flows reach very low levels around 2080–2100, reflecting a significant reduction in surface runoff.

Figure 5 also highlights an increase in interannual variability of flows under the most pessimistic scenarios. The amplitude of fluctuations becomes greater, reflecting a more pronounced alternation between relatively wet years and very dry years.

From a hydrological perspective, this annual trend in discharge reflects a gradual decline in the catchment's capacity to generate surface runoff. Several mechanisms may explain this trend: a reduction in effective precipitation, an increase in evapotranspiration due to global warming, the gradual drying out of soils, a decrease in groundwater recharge, and a reduction in baseflow. These processes act simultaneously to reduce the volumes of water available in the river system throughout the century. The catchment's response is thus becoming increasingly sensitive to future climatic conditions.

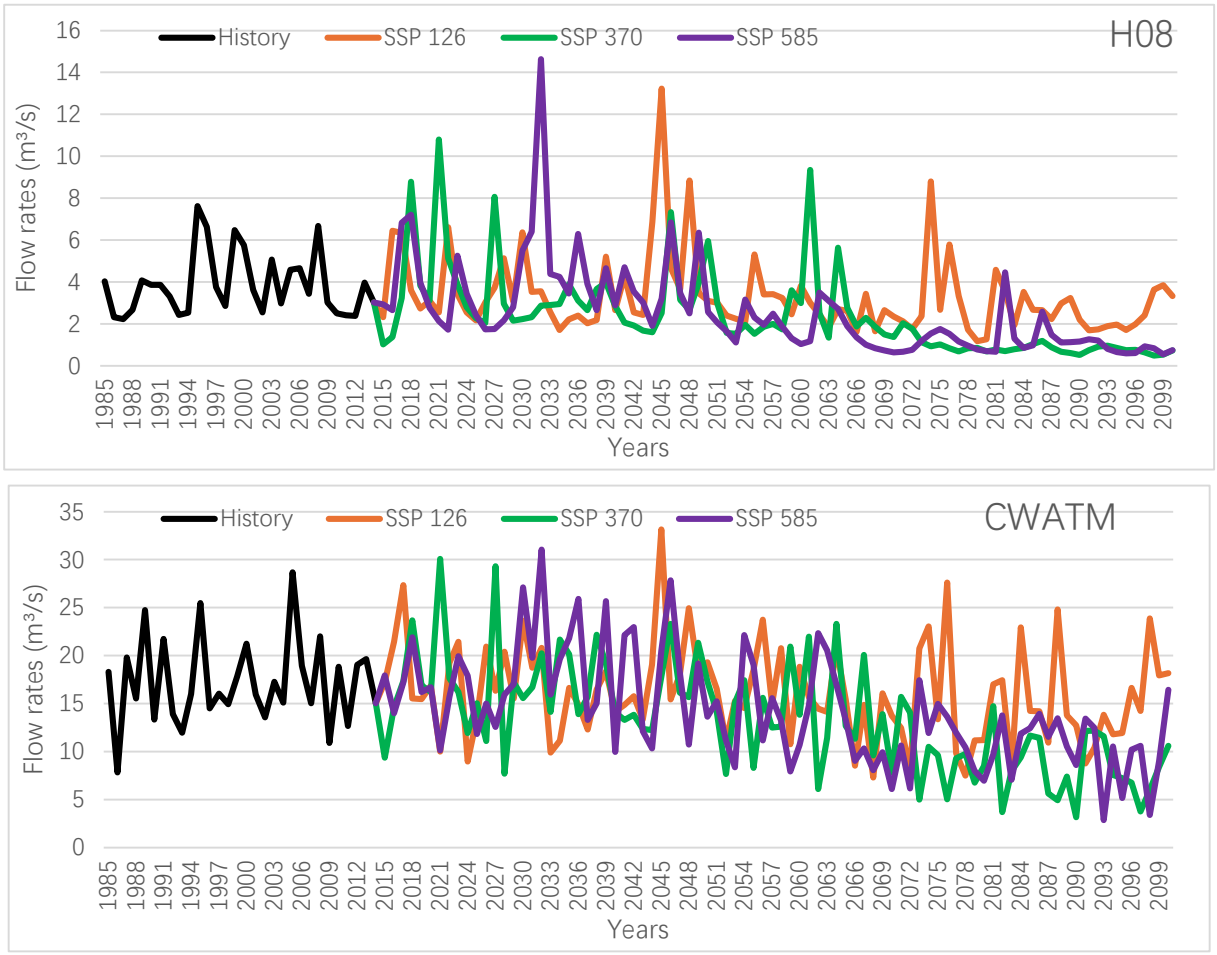


Figure 5. Trends in annual simulated runoff over the historical and future periods under the three scenarios in the Nanija Bolong catchment.

Table 4 highlights projected changes in simulated flows at the Nanija Bolong outlet. All percentage changes use the same 1985–2014 historical reference period; the table does not combine the previously inconsistent 3.97 m^3/s, 14–16 m^3/s, and 1985–2014 baselines.

Under the SSP1-2.6 scenario, corresponding to a low-emissions trajectory, changes remain relatively limited at the start of the century. Using the H08 model, the average flow rate falls from 3.97 m^3/s over the historical period (1985–2014) to 3.47 m^3/s between 2021 and 2040, representing a decrease of 12.52%. This decline is, however, followed by a temporary rebound during the period 2041–2060, when the flow rate reaches 4.37 m^3/s, representing a 10.12% increase compared with the reference period. In contrast, the subsequent periods show a more marked decrease, with 2.88 m^3/s (−27.47%) between 2061 and 2080 and 2.76 m^3/s (−30.37%) between 2081 and 2100. The CWATM model shows a comparable but less pronounced trend. Flow rates decrease from 20.0 to 18.8 m^3/s (−5.97%) between 2021 and 2040, rise slightly to 20.8 m^3/s (+4.10%) during 2041–2060, then decrease to 16.6 m^3/s (−17.10%) and 17.7 m^3/s (−11.48%) during the final two periods.

Table 4. Changes in simulated discharge from H08 and CWATM over 2021–2040, 2041–2060, 2061–2080, and 2081–2100 relative to the 1985–2014 historical reference period at the Nanija Bolong outlet.

H08	1985–20142021–2040	Trend	2041–2060	Trend	2061–2080	Trend	2081–2100	Trend
SSP 126	3.47	−12.52	4.37	10.12	2.88	−27.47	2.76	−30.37
SSP 370	3.80	−4.23	3.24	−18.3	2.16	−45.5	0.78	−80.37
SSP 585	4.31	8.55	2.77	−30.22	1.42	−64.3	1.25	−68.6
CWATM	**1985–20142021–2040**	**Trend**	**2041–2060**	**Trend**	**2061–2080**	**Trend**	**2081–2100**	**Trend**
SSP 126	18.8	−5.97	20.8	4.1	16.6	−17.1	17.7	−11.48
SSP 370	20.3	1.7	18.03	−9.9	13.49	−32.6	9.68	−51.6
SSP 585	21.0	5.1	17.7	−11.5	14.2	−29.0	12.08	−39.6

Under SSP3-7.0, the H08 simulations indicate a stronger late-century reduction than under SSP5-8.5 in the supplied ensemble results. This ordering is not inconsistent with the scenario definitions over a finite time window: runoff responds to the combined, seasonally varying changes in precipitation, evapotranspiration, soil moisture, storage, and routing, and the ensemble mean can conceal differing GCM trajectories.

Under SSP5-8.5, the projected reduction remains substantial but is smaller than under SSP3-7.0 in the selected late-century comparison for the supplied ensemble series. We therefore do not use a generic statement that the highest-emission scenario always gives the largest reduction in every period.

The four time horizons show that the magnitude and ordering of scenario responses vary through the century. The period 2021–2040 is a near-term projection window, whereas 2061–2080 and 2081–2100 show the largest long-term departures from the historical reference. Each period is interpreted with the same baseline.

CWATM consistently simulates higher discharge than H08 in the supplied series. This difference may reflect alternative representations of runoff, infiltration, storage, evapotranspiration, routing, and grid aggregation. Because there is no observation-based calibration here, the present analysis cannot determine which model is more realistic for the Nanija Bolong catchment.

3.2.2. Spatial Distribution of Annual Flows

Table 5 presents selected model grid cells or representative spatial points used to describe the spatial distribution of CWATM-simulated flows. These are not gauging stations. Point identifiers, the longitude/latitude convention, and catchment membership were checked against the catchment polygon: P1, P3, P4, and P5 are the verified 0.5° grid-cell centres retained for the analysis. The P2 coordinate could not be verified against the supplied materials and is therefore excluded from all physical interpretation. No point outside the catchment is interpreted as a catchment point.

Table 5. Selected grid cells/representative points used for the spatial distribution of CWATM-simulated flows over the historical reference period (1985–2014) and future period (2021–2100). Coordinates are longitude/latitude in decimal degrees; west longitudes are negative. The points are not observations.

Points		P1	P3	P4	P5
X		−15,130	−13,982	−15,130	−13,982
Y		13,732	13,732	14,266	14,266
History	1985–2014	74.4	42.3	51.2	16.1
SSP 126	2021–2040	71.1	40.0	41.3	15.2
	2041–2060	80.5	44.3	59.1	17.0
	2061–2080	55.3	30.2	36.7	12.7
	2081–2100	70.7	39.3	43.9	15.4
SSP 370	2021–2040	89.1	49.7	63.7	19.8
	2041–2060	87.8	47.8	62.8	19.6
	2061–2080	59.6	33.6	31.9	12.4
	2081–2100	41.8	22.6	17.6	9.9

SSP 585	2021–2040	80.1	44.5	56.5	17.0
	2041–2060	59.8	33.8	30.4	14.3
	2061–2080	62.7	35.6	32.7	13.4
	2081–2100	54.4	30.5	31.7	13.2

Figure 6 and Table 5 show spatial contrasts in the CWATM grid-cell outputs. Because the climate and hydrological products are coarse relative to the catchment, these contrasts are indicative and should not be assigned more physical detail than the grid supports.

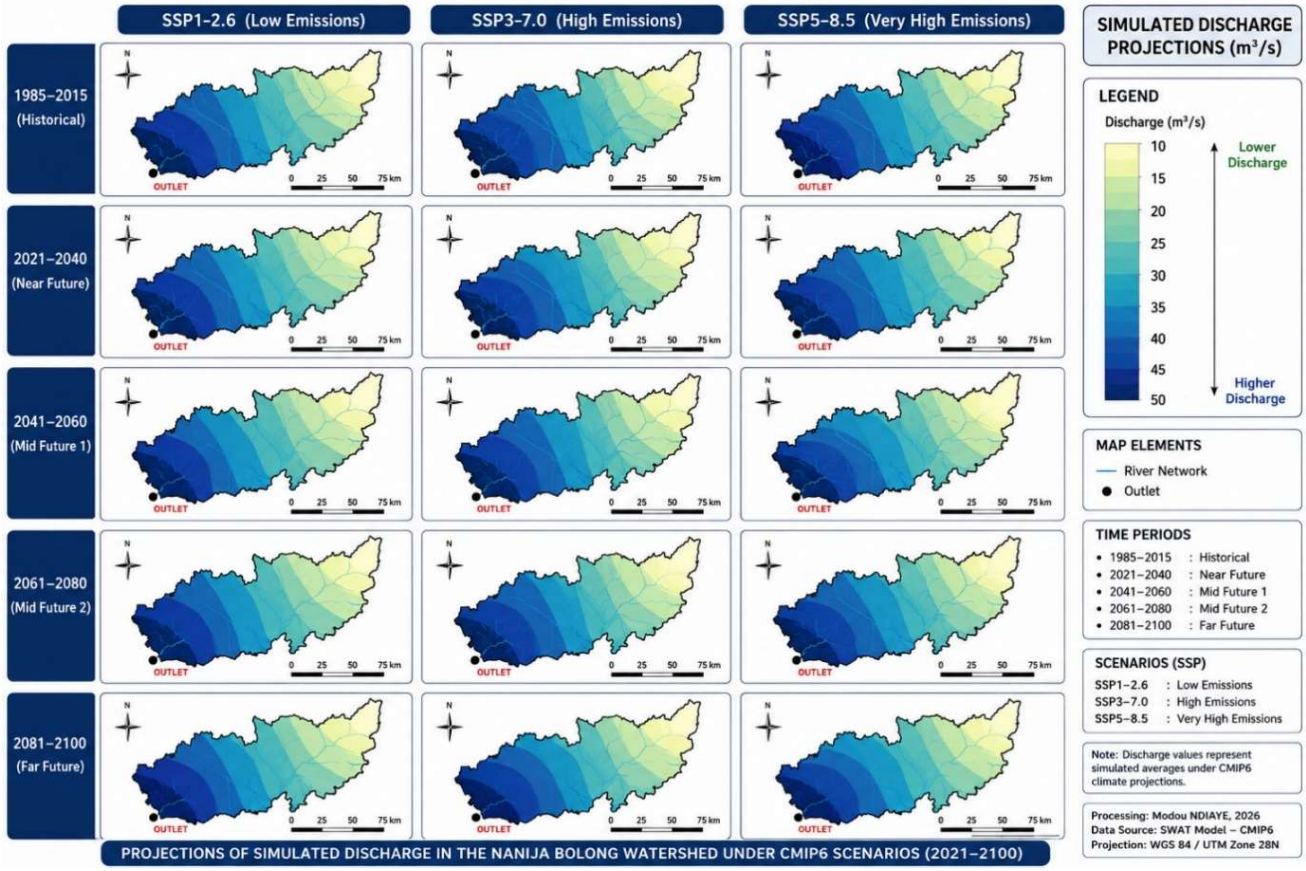


Figure 6. Spatial distribution of CWATM-simulated discharge for the historical reference period (1985–2014) and future periods (2021–2100) in the Nanija Bolong catchment. At 0.5° resolution, the map shows model-grid contrasts rather than fine-scale measured spatial patterns.

The historical spatial pattern is described only as a model-resolved contrast among selected cells. It is not interpreted as a measured southwest–northeast hydrological gradient.

Under the SSP1-2.6 scenario, changes remain relatively limited at the start of the century. Between 2021 and 2040, flow rates decrease slightly across the entire basin, falling, for example, from 74.4 to 71.1 m^3/s in the south-west (−4.4%), from 42.3 to 40.0 m^3/s in the south-east (−5.4%) and from 51.2 to 41.3 m^3/s in the north-west (−19.3%), whilst in the north-east the flow rate falls from 16.1 to 15.2 m^3/s (−5.6%). A temporary improvement then occurs between 2041 and 2060, when the flow rate reaches 80.5 m^3/s in the south-west, 59.1 m^3/s in the north-west, and 44.3 m^3/s in the south-east, before falling significantly between 2061 and 2080. The maps then show a reduction in the areas characterised by high flow rates, although the west-east gradient remains visible.

The SSP3-7.0 scenario shows the most marked contrasts. The first two periods still show relatively high flow rates, reaching 89.1 m^3/s in the south-west and 63.7 m^3/s in the north-west between 2021 and 2040. However, the situation deteriorates rapidly after 2060. Between 2081 and 2100, flow rates fall to 41.8

m^3/s in the south-west, 22.6 m^3/s in the south-east, 17.6 m^3/s in the north-west, and just 9.9 m^3/s in the north-east. Compared with the historical period, this represents a decrease of approximately 44% in the south-west, 47% in the south-east, 66% in the north-west, and 39% in the north-east. The maps in Figure 6 reflect this trend through an expansion of light colours across much of the catchment, indicating a widespread decrease in flows.

Under the SSP5-8.5 scenario, the spatial distribution remains similar, but the decreases are also significant. Discharges reach 80.1 m^3/s in the south-west in 2021–2040, then gradually decrease to 59.8 m^3/s between 2041 and 2060, 62.7 m^3/s between 2061 and 2080, and 54.4 m^3/s between 2081 and 2100. In the north-west, flows will simultaneously decrease from 56.5 to 31.7 m^3/s, whilst in the north-east they will fall from 17.0 to 13.2 m^3/s. These results show that the western sectors retain relatively higher flow rates, but are also experiencing a gradual reduction in water resources.

Overall, Figure 6 provides an indicative comparison of model-grid outputs. Higher-resolution regional or distributed modelling, supported by local observations, is needed before the spatial pattern can be used for detailed water-resource planning.

3.2.3. Monthly Trends

Figures 7 and 8, and Table 6 present the monthly trends in discharge simulated by the H08 and CWATM hydrological models for the historical period as well as for the three CMIP6 climate scenarios (SSP1-2.6, SSP3-7.0, and SSP5-8.5). Whilst Figure 7 illustrates the seasonal dynamics of flows graphically, Table 6 provides the quantitative values needed to accurately compare monthly variations between the different scenarios and time horizons. A combined analysis of these two sources helps to understand how climate change could alter the seasonality of flows in the Nanija Bolong catchment.

Table 6. Monthly changes in simulated discharge from H08 and CWATM over the historical reference period (1985–2014) and future period (2021–2100) at the Nanija Bolong outlet.

H08	**M**	**J**	**J**	**A**	**S**	**O**	**N**	**D**	**J**	**F**	**M**	**A**
History	2.22	2.07	2.47	3.12	9.03	6.94	4.62	3.99	3.44	3.05	2.73	2.45
SSP 126	1.83	1.70	2.00	2.87	9.76	4.77	3.57	3.11	2.75	2.46	2.22	2.01
SSP 370	1.40	1.29	1.32	2.45	4.82	4.46	2.62	2.28	2.06	1.85	1.68	1.53
SSP 585	1.40	1.32	1.32	1.69	6.10	4.77	2.71	2.29	2.06	1.86	1.68	1.53
CWATM	**M**	**J**	**J**	**A**	**S**	**O**	**N**	**D**	**J**	**F**	**M**	**A**
History	2.85	8.45	21.57	57.57	79.15	17.74	3.94	3.13	3.05	2.99	2.94	2.89
SSP 126	2.64	4.48	16.94	48.83	80.78	19.11	3.86	2.89	2.83	2.77	2.72	2.67
SSP 370	2.25	3.33	12.58	39.02	62.16	23.24	3.09	2.44	2.40	2.35	2.31	2.27
SSP 585	2.26	5.37	13.09	39.52	69.42	23.79	3.30	2.44	2.41	2.36	2.31	2.27

Simulations carried out using the H08 and CWATM models show that the seasonality of flows is maintained, with peak flows concentrated during the rainy season (July to October), but that the intensity and distribution of flows are changing as a result of climate change. Although the two models produce different absolute values, they both indicate a decrease in discharge over much of the year, particularly under the medium and high emissions scenarios.

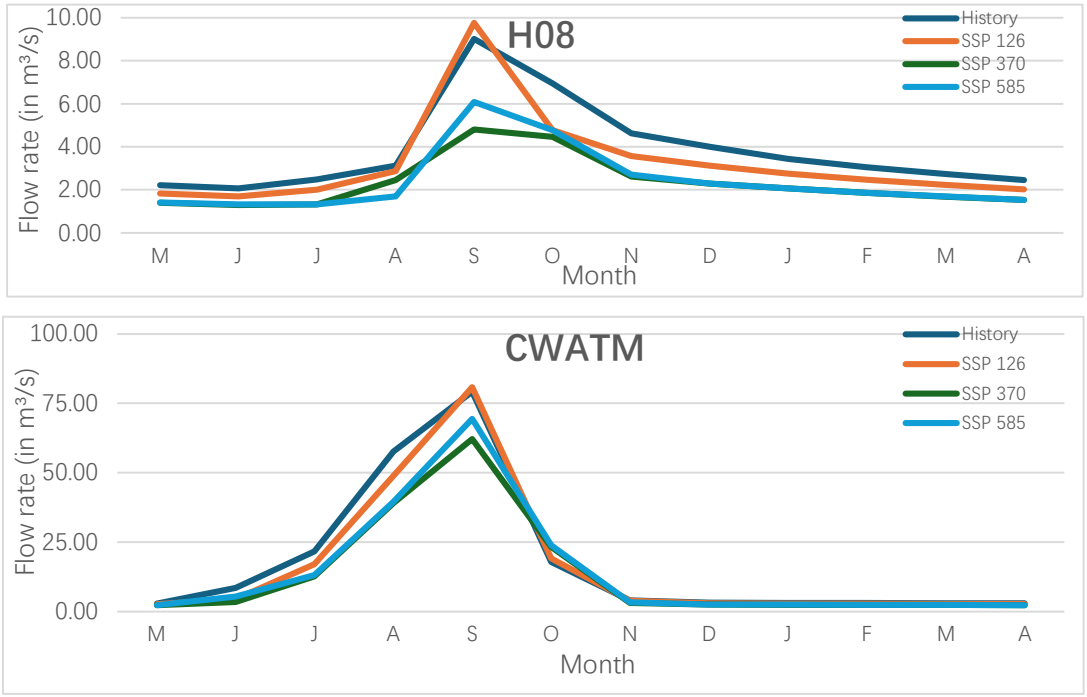


Figure 7. Monthly changes in simulated discharge from H08 and CWATM by scenario and period in the Nanija Bolong catchment. Labels identify the model and scenario directly.

Simulations using the H08 model indicate that, during the historical period, discharge rates remain low from May to August, ranging from 2.07 m^3/s in June to 3.12 m^3/s in August. Discharge increases sharply from September onwards, reaching a maximum of 9.03 m^3/s, before gradually decreasing in October (6.94 m^3/s), November (4.62 m^3/s), and December (3.99 m^3/s). This pattern reflects the typical behaviour of Sudano-Sahelian catchments, where flows are strongly influenced by the rainy season.

Under the SSP1-2.6 scenario, flow rates decrease during most months. In September, which remains the wettest month, the flow rate nevertheless rises from 9.03 to 9.76 m^3/s—a slight increase of around 8%—suggesting a temporary intensification of seasonal floods. By contrast, the other months show significant decreases, particularly in October, when the flow rate falls from 6.94 to 4.77 m^3/s (−31%), in November from 4.62 to 3.57 m^3/s (−23%), and in December from 3.99 to 3.11 m^3/s (−22%). Flow rates at the start of the season are also reduced, falling, for example, from 2.22 to 1.83 m^3/s in May.

Under the SSP3-7.0 and SSP5-8.5 scenarios, the decline becomes much more pronounced. Under SSP3-7.0, the maximum flow in September is practically halved, falling from 9.03 to 4.82 m^3/s, whilst in October it decreases from 6.94 to 4.46 m^3/s. Flows during the dry months also become very low, at just 1.29 m^3/s in June and 1.40 m^3/s in May. The SSP5-8.5 scenario shows a similar trend, although a slight increase in flow rates is observed in September (6.10 m^3/s) compared with the SSP3-7.0 scenario. However, flow rates remain well below historical levels during most months, confirming a general decline in water resources.

The results obtained using the CWATM model also highlight strong seasonality, but with much higher flows than those simulated by H08. During the historical period, flows increase rapidly between June (8.45 m^3/s) and July (21.57 m^3/s), peaking in August (57.57 m^3/s) and reaching their maximum in September at 79.15 m^3/s, before falling sharply in October (17.74 m^3/s) and then returning to values close to 3 m^3/s between November and May.

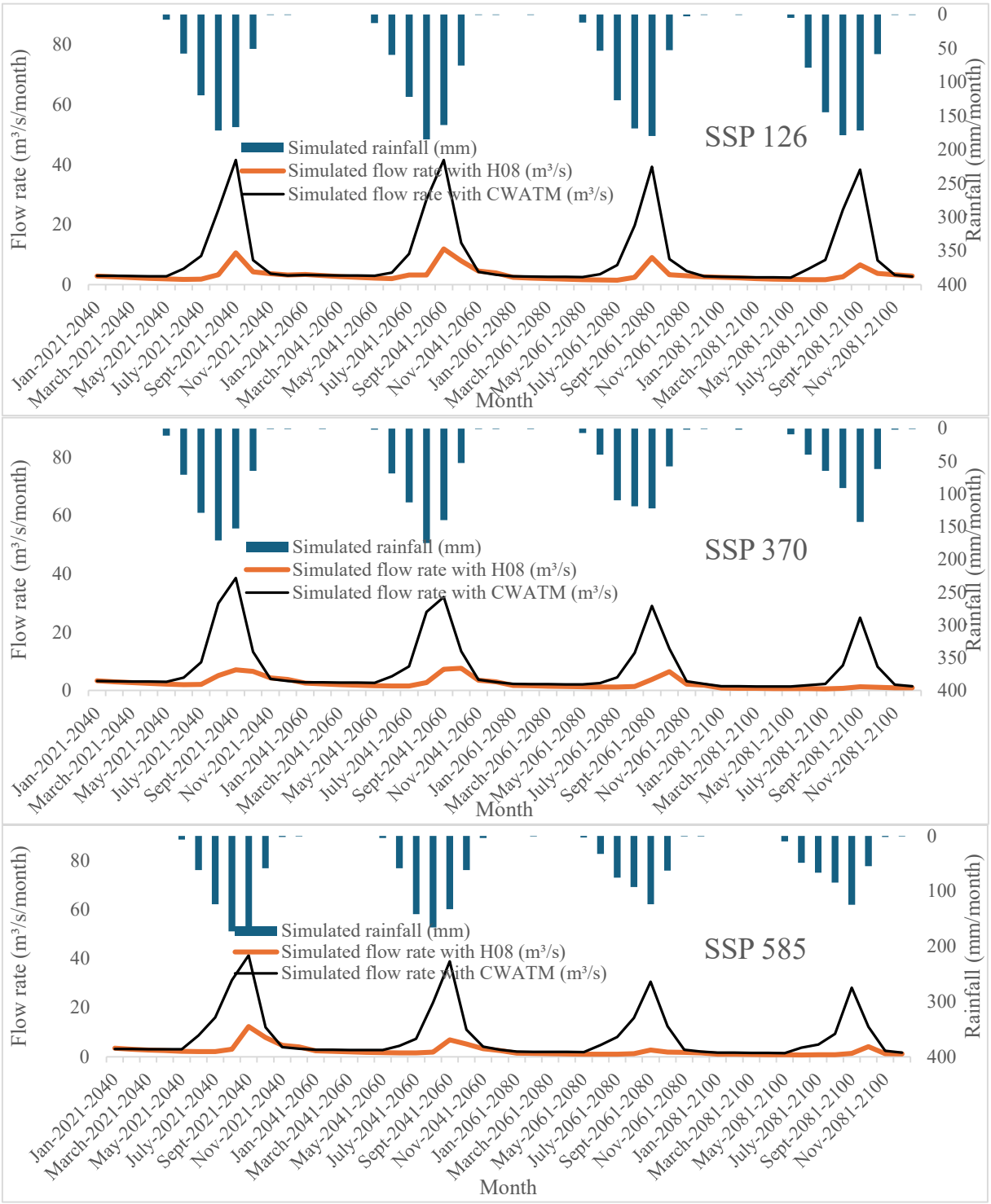


Figure 8. Monthly variation in future simulated discharge from H08 and CWATM over 2021–2100 under SSP1-2.6, SSP3-7.0, and SSP5-8.5 at the Nanija Bolong outlet. The panels are modelled projections and do not include measured discharge.

Under the SSP1-2.6 scenario, flow rates decrease during the rising water period, particularly in June (4.48 m^3/s) and July (16.94 m^3/s), whilst the September peak rises slightly to 80.78 m^3/s (+2%). This slight increase in the seasonal maximum contrasts with the decline observed during the other months, reflecting a greater concentration of flow during the flood period. The months of August and October record 48.83 m^3/s and 19.11 m^3/s, respectively, indicating a redistribution of the hydrological regime.

The SSP3-7.0 and SSP5-8.5 scenarios confirm a much more profound change in seasonal dynamics. Under SSP3-7.0, the maximum flow in September falls to 62.16 m^3/s, a decrease of around 21% compared

with the historical period, whilst in August it drops from 57.57 to 39.02 m^3/s (−32%). The SSP5-8.5 scenario presents an intermediate situation, with 69.42 m^3/s in September and 39.52 m^3/s in August. Conversely, October flows increase slightly to 23.24 m^3/s under SSP3-7.0 and 23.79 m^3/s under SSP5-8.5, suggesting a partial shift in the receding of floodwaters towards the end of the wet season.

Overall, both models show that climate change will alter the intensity of flows more than their seasonality. Flood peaks remain concentrated between August and September, but their magnitude decreases under the most pessimistic scenarios, whilst low flows become even lower during the dry season. This trend reflects a reduction in annual water availability, coupled with a concentration of flows over a shorter period. Such a change in the hydrological regime could affect groundwater recharge, the availability of water for irrigation and domestic use, aquatic ecosystems, and the management of hydraulic structures. These results highlight the need to adapt integrated water resources management strategies, taking into account the expected changes in the seasonal distribution of flows and the likely increase in hydrological variability during the 21st century.

4. Discussion

The results of this study show that the Nanija Bolong catchment is particularly vulnerable to the effects of climate change, with a gradual decline in surface water resources over the 21st century. The two hydrological models used, H08 and CWATM, converge on this same trend despite differences in the absolute values of the simulated flows, which reinforces the robustness of the projections obtained. This convergence is consistent with the recommendations of the multi-model approach developed within the ISIMIP3b framework, which aims to better represent the uncertainties associated with climate and hydrological modelling [28,32]. The differences observed between H08 and CWATM mainly reflect their respective formulations of the processes of runoff, infiltration, storage and flow routing, as previously highlighted by Hanasaki et al. [8,30] and Burek et al. [31].

The absence of a statistically significant trend in discharge during the historical period (1981–2020) confirms that the hydrological behaviour of the catchment has been dominated by natural climatic variability rather than by a sustained change in the flow regime. This observation is consistent with the analyses by Nicholson [14] and Descroix et al. [15], which show that Sudano-Sahelian basins remain strongly influenced by the alternation of wet and dry years, a legacy of the major droughts of the 1970s and 1980s and the partial recovery of rainfall since the 1990s. The breaks detected around this period, although not statistically significant, likely reflect this gradual reorganisation of the hydroclimatic regime already observed in several West African basins [46–49].

Future projections, however, reveal a marked deterioration in water resources, particularly under the SSP3-7.0 and SSP5-8.5 scenarios. The simulated decreases reach −70.3% under SSP3-7.0 and −66.2% under SSP5-8.5 with H08, compared with −42.8% and −38.6% respectively with CWATM. These results illustrate the combined effect of reduced effective precipitation, increased evapotranspiration and global warming, in line with the conclusions of the IPCC [1], which predicts an intensification of the hydrological cycle accompanied by a reduction in water availability in several tropical and subtropical regions [50,51]. They are also consistent with research carried out in Senegal and West Africa by Dione and Faye [36] and Sadio et al. [39,40], which highlight a gradual decline in flow rates in the Agua-Foua-Djilass, Casamance and Kayanga catchment areas under the most pessimistic climate scenarios.

The strong seasonality of runoff observed in this study confirms that the hydrological regime of the Nanija Bolong remains primarily controlled by the winter rainy season. The simulations, however, show a greater concentration of runoff over a shorter period, with more irregular flood peaks and a significant decrease in dry-season flows. This trend is consistent with the observations of Panthou et al. [16], who report an increase in extreme rainfall events in West Africa, as well as with the analyses by Arnell and Gosling [52] showing that climate change alters the temporal distribution of runoff more significantly than

its mere annual volume. The rise in temperatures observed in Senegal since the 1990s [53] is likely to increase potential evapotranspiration, further reducing available flow rates.

Finally, these findings highlight the need to incorporate hydroclimatic projections into integrated water resources management policies for the Nanija Bolong catchment [54]. The projected declines could jeopardise irrigation, drinking water supplies, agro-pastoral activities and the functioning of aquatic ecosystems [55]. Adaptation measures based on the development of hillside reservoirs, improving irrigation efficiency, restoring vegetation cover, protecting groundwater recharge areas and strengthening hydroclimatic monitoring systems appear essential. These recommendations are in line with the approaches advocated by Krysanova and White [56], Arnold et al. [57] and the IPCC [1], who regard planning based on climate projections as a key lever for strengthening the resilience of catchment areas to climate change. Furthermore, the hydrological modelling and evaluation approaches discussed by Rathnayake et al. [58,59] underscore the importance of assessing model performance against observed discharge data and accounting for modelling uncertainties to improve the reliability of hydrological projections and support evidence-based water resources management.

5. Conclusions

This study assessed model-simulated historical and future runoff in the Nanija Bolong catchment using H08 and CWATM driven by three CMIP6 climate models. The common historical reference period was 1985–2014, and projections covered 2021–2100. Both hydrological models indicate substantial uncertainty in absolute runoff, while future changes vary with the model, climate forcing, and scenario. The spread across the three climate models is now explicitly quantified for the historical period (Table 1: mean ± SD and max–min range), and the future ensemble results are interpreted together with this uncertainty.

The principal result is a projected long-term reduction in simulated runoff in several scenario-period combinations, with especially large reductions in the supplied late-century SSP3-7.0 ensemble series. Because SSP3-7.0 and SSP5-8.5 do not have a strictly monotonic ordering in every selected period, the scenario results are interpreted as period-specific projections rather than a simple ranking by emissions level.

The study does not provide observational validation as there are no observed discharges in the Nanija Bolong basin. The rainfall–simulated-flow relationships and agreement between H08 and CWATM should not be confused with measured-versus-modelled performance. The coarse spatial resolution also limits the interpretation of within-catchment patterns.

The results support the use of local observations, higher-resolution modelling and explicit uncertainty analysis in future work. Storage, recharge protection, and irrigation measures are candidate management options, not interventions tested by this study; their effectiveness must be evaluated separately.

Data Availability Statement. The model-derived time series and processing workbook used in this analysis are available from the authors upon reasonable request. Any observed discharge series used in a future validation must be archived with station metadata, units, quality-control information, the outlet definition, and the extraction procedure.

Statement of the Use of Generative AI and AI-Assisted Technologies in the Writing Process

During the preparation of this manuscript, the authors used ChatGPT (OpenAI) to assist with the calculation and verification of certain statistical parameters, as well as the formatting, linguistic refinement, and editorial organization of the manuscript. After using this tool, the authors carefully reviewed and verified the statistical results, revised and edited the content as needed, and take full responsibility for the accuracy, scientific integrity, and content of the published article.

Acknowledgments

The authors would like to express their gratitude to the institutions and research initiatives that facilitate access to climate and hydrological data, particularly the Inter-Sectoral Impact Model Intercomparison Project (ISIMIP) and the Coupled Model Intercomparison Project Phase 6 (CMIP6). The availability of these datasets and hydrological model outputs was essential for conducting this study. The authors also acknowledge the technical and institutional support provided by the Geomatics and Environment Laboratory, Department of Geography, Assane Seck University of Ziguinchor, Senegal. The authors are grateful to all individuals and institutions whose contributions facilitated the preparation and completion of this research.

Author Contributions

M.N. and C.F. conceptualized the study, conducted the data analysis, interpreted the results, and wrote, reviewed, and edited the manuscript. Both authors have read and approved the final manuscript.

Ethics Statement

Not applicable for studies not involving humans or animals.

Informed Consent Statement

Not applicable for studies not involving humans.

Data Availability Statement

The hydrological and climate projection data used in this study are available from the ISIMIP project repository (https://www.isimip.org, accessed on 5 February 2026). The datasets analysed during the current study are available from the corresponding author on reasonable request.

Funding

This research did not receive any specific grant from funding agencies in the public, commercial, or not-for-profit sectors.

Declaration of Competing Interest

The authors declare that they have no known competing financial interests or personal relationships that could have appeared to influence the work reported in this paper.

References

1. IPCC. *Climate Change 2023: Synthesis Report. Contribution of Working Groups I, II and III to the Sixth Assessment Report of the Intergovernmental Panel on Climate Change*; IPCC: Geneva, Switzerland, 2023.
2. Oreskes N. The Scientific Consensus on Climate Change. *Science* **2004**, *306*, 1686–1686. DOI:10.1126/science.1103618
3. Marotzke J, Jakob C, Bony S, Dirmeyer PA, O'Gorman PA, Hawkins E, et al. Climate research must sharpen its view. *Nat. Clim. Change* **2017**, *7*, 89–91. DOI:10.1038/nclimate3206
4. Bierkens MFP. Global hydrology 2015: State, trends, and directions. *Water Resour. Res.* **2015**, *51*, 4923–4947. DOI:10.1002/2015WR017173
5. Haddeland I, Heinke J, Biemans H, Eisner S, Flörke M, Hanasaki N, et al. Global water resources affected by human interventions and climate change. *Proc. Natl. Acad. Sci. USA* **2014**, *111*, 3251–3256. DOI:10.1073/pnas.1222475110
6. Döll P, Jiménez-Cisneros B, Oki T, Arnell NW, Benito G, Cogley JG, et al. Integrating risks of climate change into water management. *Hydrol. Sci. J.* **2015**, *60*, 4–13. DOI:10.1080/02626667.2014.967250
7. Moradkhani H, Sorooshian S. General review of rainfall-runoff modeling: Model calibration, data assimilation, and uncertainty analysis. In *Hydrological Modelling and the Water Cycle: Coupling the Atmospheric and Hydrological Models*;

Sorooshian S, Hsu K-L, Coppola E, Tomassetti B, Verdecchia M, Visconti G, Eds.; Springer: Berlin/Heidelberg, Germany, 2008; pp. 1–24. DOI:10.1007/978-3-540-77843-1_1

8. Hanasaki N, Kanae S, Oki T, Masuda K, Motoya K, Shirakawa N, et al. An integrated model for the assessment of global water resources—Part 1: Model description and input meteorological forcing. *Hydrol. Earth Syst. Sci.* **2008**, *12*, 1007–1025. DOI:10.5194/hess-12-1007-2008
9. Pokhrel YN, Hanasaki N, Wada Y, Kim H. Recent progresses in incorporating human land–water management into global land surface models toward their integration into Earth system models. *WIREs Water* **2016**, *3*, 548–574. DOI:10.1002/wat2.1150
10. Sutanudjaja EH, van Beek R, Wanders N, Wada Y, Bosmans JHC, Drost N, et al. PCR-GLOBWB 2: A 5 arcmin global hydrological and water resources model. *Geosci. Model Dev.* **2018**, *11*, 2429–2453. DOI:10.5194/gmd-11-2429-2018
11. Dessu SB, Melesse AM. Impact and uncertainties of climate change on the hydrology of the Mara River basin, Kenya/Tanzania. *Hydrol. Process.* **2013**, *27*, 2973–2986. DOI:10.1002/hyp.9434
12. Bekele D, Alamirew T, Kebede A, Zeleke G, Melesse AM. Modeling Climate Change Impact on the Hydrology of Keleta Watershed in the Awash River Basin, Ethiopia. *Environ. Model. Assess.* **2019**, *24*, 95–107. DOI:10.1007/s10666-018-9619-1
13. Mendez M, Calvo-Valverde LA, Imbach P, Maathuis B, Hein-Grigg D, Hidalgo-Madriz JA, et al. Hydrological Response of Tropical Catchments to Climate Change as Modeled by the GR2M Model: A Case Study in Costa Rica. *Sustainability* **2022**, *14*, 16938. DOI:10.3390/su142416938
14. Nicholson SE. The West African Sahel: A Review of Recent Studies on the Rainfall Regime and Its Interannual Variability. *ISRN Meteorol.* **2013**, *2013*, 453521. DOI:10.1155/2013/453521
15. Descroix L, Guichard F, Grippa M, Lambert LA, Panthou G, Mahé G, et al. Evolution of Surface Hydrology in the Sahelo-Sudanian Strip: An Updated Review. *Water* **2018**, *10*, 748. DOI:10.3390/w10060748
16. Panthou G, Lebel T, Vischel T, Quantin G, Sane Y, Ba A, et al. Rainfall intensification in tropical semi-arid regions: The Sahelian case. *Environ. Res. Lett.* **2018**, *13*, 064013. DOI:10.1088/1748-9326/aac334
17. Kandji ST, Verchot L, Mackensen J. *Climate Change and Variability in Southern Africa: Impacts and Adaptation in the Agricultural Sector*; United Nations Environment Programme (UNEP): Nairobi, Kenya, 2006.
18. Klutse NAB, Quagraine KA, Nkrumah F, Quagraine KT, Berkoh-Oforiwaa R, Dzrobi JF, et al. The Climatic Analysis of Summer Monsoon Extreme Precipitation Events over West Africa in CMIP6 Simulations. *Earth Syst. Environ.* **2021**, *5*, 25–41. DOI:10.1007/s41748-021-00203-y
19. ANACIM. *Cadre national de services climatologiques: Bulletin agrométéorologique, deuxième décade d'août 2023*; Agence Nationale de l'Aviation Civile et de la Météorologie: Dakar, Sénégal, 2023.
20. Bodian A. Caractérisation de la variabilité hydroclimatique et de ses impacts sur les ressources en eau en Afrique de l'Ouest: Étude de cas des bassins de la Gambie et de la Casamance. Ph.D. Thesis, Université Cheikh Anta Diop de Dakar, Dakar, Sénégal, 2014.
21. Sanoussi A, Mohamed L, Seyni S, David AG. Adapting to climate variability and change in smallholder farming communities: A case study from Burkina Faso, Chad and Niger. *J. Agric. Ext. Rural. Dev.* **2015**, *7*, 16–27. DOI:10.5897/JAERD14.0595
22. Alaghmand S, Beecham S, Hassanli A. Impacts of Vegetation Cover on Surface-Groundwater Flows and Solute Interactions in a Semi-Arid Saline Floodplain: A Case Study of the Lower Murray River, Australia. *Environ. Process.* **2014**, *1*, 59–71. DOI:10.1007/s40710-014-0003-0
23. Shadmehri Toosi A, Calbimonte GH, Nouri H, Alaghmand S. River basin-scale flood hazard assessment using a modified multi-criteria decision analysis approach: A case study. *J. Hydrol.* **2019**, *574*, 660–671. DOI:10.1016/j.jhydrol.2019.04.072
24. OMVS. *Plan d'Action GIRE du Bassin Versant du Fleuve Kayanga/Géba. Volume 3: Portfolio de Projets*; Facilité Africaine de l'Eau: Abidjan, Côte d'Ivoire, 2012; 125p.
25. Eyring V, Bony S, Meehl GA, Senior CA, Stevens B, Stouffer RJ, et al. Overview of the Coupled Model Intercomparison Project Phase 6 (CMIP6) experimental design and organization. *Geosci. Model Dev.* **2016**, *9*, 1937–1958. DOI:10.5194/gmd-9-1937-2016
26. The CMIP6 landscape. *Nat. Clim. Change* **2019**, *9*, 727. DOI:10.1038/s41558-019-0599-1
27. Frieler K, Lange S, Piontek F, Reyer CPO, Schewe J, Warszawski L, et al. Assessing the impacts of 1.5 °C global warming—Simulation protocol of the Inter-Sectoral Impact Model Intercomparison Project (ISIMIP2b). *Geosci. Model Dev.* **2017**, *10*, 4321–4345. DOI:10.5194/gmd-10-4321-2017
28. Lange S. Trend-preserving bias adjustment and statistical downscaling with ISIMIP3BASD (v1.0). *Geosci. Model Dev.* **2019**, *12*, 3055–3070. DOI:10.5194/gmd-12-3055-2019
29. Babaousmail H, Hou R, Ayugi B, Ojara M, Ngoma H, Karim R, et al. Evaluation of the Performance of CMIP6 Models in Reproducing Rainfall Patterns over North Africa. *Atmosphere* **2021**, *12*, 475. DOI:10.3390/atmos12040475

30. Hanasaki N, Fujiwara M, Maji A, Seto S. On the Applicability of the H08 Global Water Resources Model to the Kyusyu Island. *J. Jpn. Soc. Civ. Eng.* **2018**, *74*, I_109–I_114. DOI:10.2208/jscejhe.74.I_109
31. Burek P, Satoh Y, Kahil T, Tang T, Greve P, Smilovic M, et al. Development of the Community Water Model (CWatM v1.04)—A high-resolution hydrological model for global and regional assessment of integrated water resources management. *Geosci. Model Dev.* **2020**, *13*, 3267–3298. DOI:10.5194/gmd-13-3267-2020
32. Thober S, Kumar R, Wanders N, Marx A, Pan M, Rakovec O, et al. Multi-model ensemble projections of European river floods and high flows at 1.5, 2, and 3 degrees global warming. *Environ. Res. Lett.* **2018**, *13*, 014003. DOI:10.1088/1748-9326/aa9e35
33. Broderick C, Murphy C, Wilby RL, Matthews T, Prudhomme C, Adamson M. Using a Scenario-Neutral Framework to Avoid Potential Maladaptation to Future Flood Risk. *Water Resour. Res.* **2019**, *55*, 1079–1104. DOI:10.1029/2018WR023623
34. Ahmad I, Tang D, Wang T, Wang M, Wagan B. Precipitation Trends over Time Using Mann-Kendall and Spearman's rho Tests in Swat River Basin, Pakistan. *Adv. Meteorol.* **2015**, *2015*, 431860. DOI:10.1155/2015/431860
35. Girma E, Tino J, Wayessa G. Rainfall trend and variability analysis in Setema-Gatira area of Jimma, Southwestern Ethiopia. *Afr. J. Agric. Res.* **2016**, *11*, 3037–3045. DOI:10.5897/AJAR2015.10160
36. Dione PM, Faye C. Assessment of the Impact of Climate Change on Current and Future Flow in the Agua-Foua-Djilass Watershed Using the CWatM Model under ISIMIP. In *2nd International Korkut Ata Scientific Researches Conference*; Kardaşlar A, Mike F, Eds.; IKSAD Publications: Ankara, Türkiye, 2023; pp. 346–369.
37. Dione PM, Faye C, Sadio CAAS. Hydrological Impacts of Climate Change (Rainfall and Temperature) and Characterization of Future Drought in the Aga Foua Djilas Watershed. *Indones. J. Soc. Environ. Issues* **2023**, *4*, 353–375. DOI:10.47540/ijsei.v4i3.1218
38. Sadio CAAS, Faye C. Evaluation of extreme flow characteristics in the Casamance watershed upstream of Kolda using the IHA/RVA method. *Int. J. Sustain. Energy Environ. Res.* **2023**, *12*, 31–45. DOI:10.18488/13.v12i2.3584
39. Sadio CAAS, Faye C, Pande CB, Tolche AD, Ali MS, Cabral-Pinto MMS, et al. Hydrological response of tropical rivers basins to climate change using the GR2M model: The case of the Casamance and Kayanga-Géva rivers basins. *Environ. Sci. Eur.* **2023**, *35*, 113. DOI:10.1186/s12302-023-00822-4
40. Sadio CAAS, Faye C, Dione PM. Impacts of Climate Change on Meteorological and Hydrological Drought in the Casamance Basin in Kolda and the Kayanga Basin in Wassadou. *J. Mater. Environ. Sci.* **2024**, *15*, 83–115. Available online: https://www.jmaterenvironsci.com/Document/vol15/vol15_N1/JMES-2024-150106-Sadio.pdf (accessed on 30 February 2026).
41. Séne SMK, Faye C. Extreme Dry and Wet Events in the Gambia River Basin Estimated for the 21st Century on the Basis of SPI Calculated from Climate Projections. In Proceedings of the 6th International Piri Reis Conference on Linguistic, History & Geography, Ganja, Azerbaijan, 14–15 November 2023; pp. 108–132.
42. Séne SMK, Faye C, Pande CB. Assessment of current and future trends in water resources in the Gambia River Basin in a context of climate change. *Environ. Sci. Eur.* **2024**, *36*, 32. DOI:10.1186/s12302-024-00848-2
43. Gudmundsson L, Brunner MI, Döll P, Fluet-Chouinard E, Frolova N, Gosling SN, et al. Past and future change in global river flows. *Nat. Rev. Earth Environ.* **2026**, *7*, 7–23. DOI:10.1038/s43017-025-00745-z
44. Mbaye ML, Ndiaye A, Coppola E. Multi-model assessment of present and future mean and extreme river flows in major West African basins. *Sci. Afr.* **2026**, *32*, e03374. DOI:10.1016/j.sciaf.2026.e03374
45. Adeyeri OE. Hydrology and Climate Change in Africa: Contemporary Challenges, and Future Resilience Pathways. *Water* **2025**, *17*, 2247. DOI:10.3390/w17152247
46. Bogning S, Frappart F, Mahé G, Niño F, Paris A, Sihon J, et al. Variations hydrologiques à long terme du bassin de l'Ogooué. In *Hydrologie, Climat et Biogéochimie du Bassin du Congo: Une Base pour l'Avenir*; American Geophysical Union: Washington, DC, USA, 2022; pp. 375–399.
47. Obahoundje S, Diedhiou A, Kouassi KL, Ta MY, Mortey EM, Roudier P, et al. Analysis of hydroclimatic trends and variability and their impacts on hydropower generation in two river basins in Côte d'Ivoire (West Africa) during 1981–2017. *Environ. Res. Commun.* **2022**, *4*, 065001. DOI:10.1088/2515-7620/ac71fa
48. Dibi-Anoh PA, Koné M, Gerdener H, Kusche J, N'Da CK. Hydrometeorological Extreme Events in West Africa: Droughts. *Surv. Geophys.* **2023**, *44*, 173–195. DOI:10.1007/s10712-022-09748-7
49. Fowé T, Yonaba R, Konaté MT, Mounirou LA, Nkiaka E, Karambiri H. A 60-year analysis of past hydroclimatic variability and trends in the Mouhoun river catchment in West Africa. *Sci. Rep.* **2025**, *15*, 21358. DOI:10.1038/s41598-025-06549-x
50. Ficklin DL, Null SE, Abatzoglou JT, Novick KA, Myers DT. Hydrological Intensification Will Increase the Complexity of Water Resource Management. *Earth's Future* **2022**, *10*, e2021EF002487. DOI:10.1029/2021EF002487

51. Banda VD, Dzwairo RB, Singh SK, Kanyerere T. Hydrological Modelling and Climate Adaptation under Changing Climate: A Review with a Focus in Sub-Saharan Africa. *Water* **2022**, *14*, 4031. DOI:10.3390/w14244031
52. Arnell NW, Gosling SN. The impacts of climate change on river flow regimes at the global scale. *J. Hydrol.* **2013**, *486*, 351–364. DOI:10.1016/j.jhydrol.2013.02.010
53. Diallo F. Variabilité et Changement Hydro-Climatiques dans le Bassin Versant de la Sandougou (Sénégal). Master's Thesis, Département de Physique, Université Assane Seck de Ziguinchor, Ziguinchor, Senegal, 2025.
54. Chiew FH, Zheng H, Potter NJ, Charles SP, Thatcher M, Ji F, et al. Different Hydroclimate Modelling Approaches Can Lead to a Large Range of Streamflow Projections under Climate Change: Implications for Water Resources Management. *Water* **2022**, *14*, 2730. DOI:10.3390/w14172730
55. Muzammal H, Zaman M, Safdar M, Adnan Shahid M, Sabir MK, Khil A, et al. Climate Change Impacts on Water Resources and Implications for Agricultural Management. In *Transforming Agricultural Management for a Sustainable Future: Climate Change and Machine Learning Perspectives*; Springer Nature Switzerland: Cham, Switzerland, 2024; pp. 21–45.
56. Krysanova V, White M. Advances in water resources assessment with SWAT—An overview. *Hydrol. Sci. J.* **2015**, *60*, 771–783. DOI:10.1080/02626667.2015.1029482
57. Arnold JG, Moriasi DN, Gassman PW, Abbaspour KC, White MJ, Srinivasan R, et al. SWAT: Model Use, Calibration, and Validation. *Trans. ASABE* **2012**, *55*, 1491–1508. DOI:10.13031/2013.42256
58. Rathnayake N, Rathnayake U, Chathuranika I, Dang TL, Hoshino Y. Cascaded-ANFIS to simulate nonlinear rainfall–runoff relationship. *Appl. Soft Comput.* **2023**, *147*, 110722. DOI:10.1016/j.asoc.2023.110722
59. Rathnayake N, Rathnayake U, Dang TL, Hoshino Y. Water level prediction using soft computing techniques: A case study in the Malwathu Oya, Sri Lanka. *PLoS ONE* **2023**, *18*, e0282847. DOI:10.1371/journal.pone.0282847